actuators

MDPI

Article

A Reasoned Attempt to Mitigate Vibrations in Nonlinear Flexible Systems Influenced by Tractive–Elastic Rolling Contact Friction Through Input Shaping: A Case Study on a Trolley–Pipe Benchmark Transport System

Gerardo Peláez [1,*,†,‡], Pablo Izquierdo [1,‡], Gustavo Peláez [2,‡] and Higinio Rubio [3,‡]

[1] Department of Mechanical Engineering, Universidade de Vigo, 36310 Pontevedra, Spain; pabloizquierdob@uvigo.es
[2] Department of Desing and Manufacturing, University of Vigo, 36208 Vigo, Spain; gupelaez@uvigo.es
[3] Department of Mechanical Engineering, Universidad Carlos III de Madrid, 28903 Madrid, Spain; hrubio@ing.uc3.es
* Correspondence: gpelaez@uvigo.es; Tel.: +34-986-811964
† Current address: School of Industrial Engineering, Lagoas-Marcosende, 36310 Vigo, Spain.
‡ These authors contributed equally to this work.

Abstract: The well-regarded feedforward control strategy known as Input Shaping is aimed at improving the dynamic response of flexible mechanical systems by reducing overshoot and residual vibration amplitude. Its validity has been confirmed by numerous studies dealing with linear system dynamics. However, its application in nonlinear systems, particularly those influenced by tractive–elastic rolling contact friction, remains a challenging and less explored open research area. This paper investigates whether Input Shaping, without tractive rolling friction compensation, can effectively mitigate vibrations in a trolley–pipe benchmark transport system. In this system, the pipe is modeled as a rolling disc attached to the trolley by a spring at its center of mass, while the trolley itself is connected to a guiding body frame by an additional spring acting as a proportional control. The natural frequencies of the system are analytically estimated and numerically verified from a corresponding well-suited multibody model. Thus, tailored two-mode shapers are designed based on simultaneous constraints and the convolution sum, respectively. Through multibody simulations, this study evaluates the performance of Input Shaping under tractive–elastic rolling contact friction conditions. The findings highlight both the potential and limitations of this control method in addressing nonlinear mechanical systems influenced by tractive–elastic rolling contact friction.

Keywords: input shaping; tractive–elastic rolling contact friction; multibody dynamics; nonlinear systems; flexible systems; dynamic friction compensation

check for updates

Academic Editors: Nan Wu, Zeqi Lu and Hailing Fu

Received: 2 January 2025
Revised: 1 February 2025
Accepted: 8 February 2025
Published: 17 February 2025

Citation: Peláez, G.; Izquierdo, P.; Peláez, G.; Rubio, H. A Reasoned Attempt to Mitigate Vibrations in Nonlinear Flexible Systems Influenced by Tractive–Elastic Rolling Contact Friction Through Input Shaping: A Case Study on a Trolley–Pipe Benchmark Transport System. *Actuators* **2025**, *14*, 97. https://doi.org/10.3390/act14020097

Copyright: © 2025 by the authors. Licensee MDPI, Basel, Switzerland. This article is an open access article distributed under the terms and conditions of the Creative Commons Attribution (CC BY) license (https://creativecommons.org/licenses/by/4.0/).

1. Introduction

1.1. Motivation

Input Shaping is a feedforward control technique designed to reduce or eliminate residual vibrations in flexible mechanical systems. Its origins can be traced back to the Posicast Control developed by O. J. Smith in 1957, which laid the groundwork for addressing transient oscillations in dynamic systems [1]. In the early 1990s, Neil Singer and Warren Seering further developed this idea, refining it into what is now widely recognized as Input Shaping [2]. Since then, William Singhose, a Ph.D. student of Seering's, has become one of

the most prolific contributors to this field, publishing extensively on its applications and methodologies [3].

Over the years, Input Shaping has proven to be a versatile and robust control strategy, with successful implementations in a wide range of applications. These include experimental studies conducted during the NASA Shuttle Program [4] as well as practical applications in overhead cranes, flexible manipulators, and linear mechanical systems in Transportation Engineering [5].

The process of shaping an input command involves convolving the original command with the selected input shaper. Typical input shapers include the Zero Vibration (ZV) shaper and the Zero Vibration and Derivative (ZVD) shaper. The ZV shaper, comprising only two coefficients, ensures that the residual vibration caused by a sequence of autocancelling impulses is entirely eliminated. In contrast, the ZVD shaper, by including additional constraints, nullifies not only the residual vibration but also its first derivative, providing enhanced robustness to the modeling of inaccuracies and frequency estimation errors.

Figure 1 demonstrates this operation using a ZV filter applied to a step input command. The velocity command before and after shaping is shown, along with the corresponding payload response. The shaped command smooths out abrupt transitions, redistributing the input energy to mitigate vibratory effects. As a result, the residual vibration in the payload response is significantly reduced, underscoring the effectiveness of the ZV shaper.

Despite its effectiveness in linear systems, extending Input Shaping to nonlinear systems presents significant challenges. Heckman and J. Lawrence, students of Singhose, made early attempts to apply Input Shaping to systems with Coulomb friction under gross-sliding conditions. Their work used compensators to linearize the system, achieving moderate success [6]. However, the application of Input Shaping to systems with tractive–elastic rolling contact friction is far more complex due to the nonlinearity introduced by the directional dependency of such friction's force on multibody system accelerations.

This study builds on the foundational work in the field and investigates the application of Input Shaping to nonlinear systems characterized by tractive–elastic rolling contact friction. The unique challenges posed by this friction resistance type highlight the need for innovative approaches to extend the benefits of Input Shaping beyond linear scenarios.

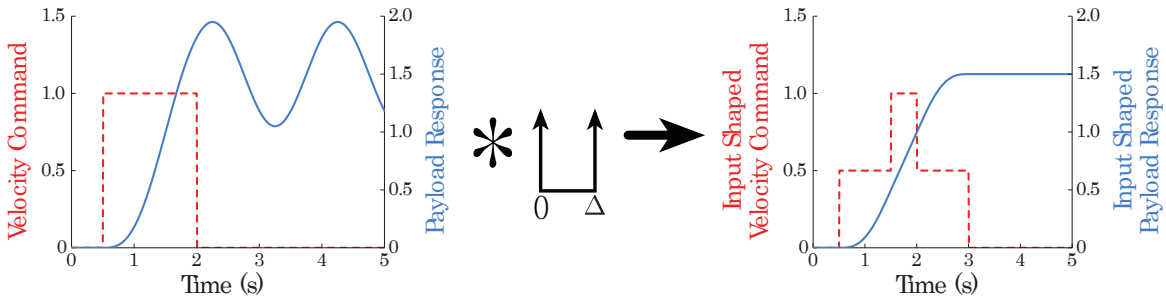

Figure 1. Application Unshaped and ZV-filtered responses to a step input: The unshaped input and its corresponding response are shown on the left, while the shaped input and the resulting vibration-suppressed response appear on the right.

It is the purpose of this primary study on the subject to describe how tractive–elastic rolling contact frictional effects in flexible systems affect Input Shaping performances and how to overcome them.

1.2. Background: Previous Works

Command generation techniques that reduce vibration and compensate for gross-sliding friction were investigated in [7]. Figure 2 illustrates two representations of a

mass-spring-damper nonlinear system undergoing gross-sliding friction. Figure 2a depicts the benchmark mechanical–physical representation composed of a mass m which moves horizontally, a spring with stiffness K_p that applies a restoring force proportional to the displacement x, and a damping element with coefficient K_D which resists motion proportional to velocity; lumped together, these become a PD-control for the system displacement x as a result of the input motion r fed by an external command generator. Note that the mass displacement is influenced by nonlinear gross-sliding friction $-sign(\dot{x})\mu_k mg$, where $\mu_k mg$ is the magnitude of the friction force and $-sign\dot{x}$ denotes its direction. The system models real-world dynamics where frictional forces cause resistance in motion by gross sliding, modeled by the kinetic friction coefficient μ_k. Regarding Figure 2b, i.e., the block diagram representation, this provides a mathematical equivalent of the physical system: the input signal r represents the desired position, and the signal is compared to the current position x to generate the error. A block containing the spring K_p and damping K_D characteristics of a PD-control process the error. The nonlinear gross-sliding friction block $-sing(\dot{x})\mu_k mg$ adds a force opposing the motion, making the system nonlinear. The plant block $\frac{1}{ms^2}$ represents the dynamics of the mass, where acceleration integrates to velocity and position. The flow of signals through the blocks models the interaction of forces, and the term $-sing(\dot{x})\mu_k mg$ introduces nonlinearity, making the system behavior more complex compared to the purely linear mass-spring-damper system, and it is given by

$$m\ddot{x} + K_D\dot{x} + K_P x = K_D\dot{r} + K_P r - sing(\dot{x})\mu_k N \tag{1}$$

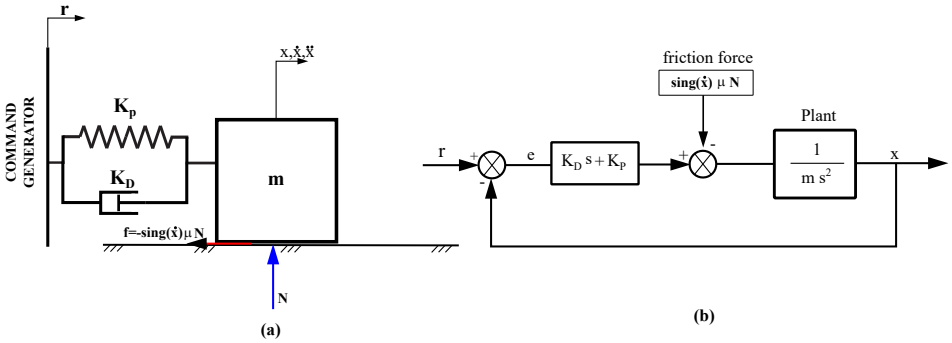

Figure 2. (**a**) Physical representation of the mass-spring-damper system under gross-sliding friction force. (**b**) Block diagram representation of the system dynamics by the Laplace model.

Many texts [8,9] provide an analytical solution for the system represented in Figure 1. Without including the derivative action of the damper, that is, if the only damping considered is the one caused by Coulomb friction in gross slip, then the decrease in vibration amplitude is not logarithmic -as in the case of viscous damping proportional to velocity- but linear, as depicted in Figure 3. In the literature [8,9], it is demonstrated that its value is given by

$$X_{n+1} = X_n - \frac{4\mu N}{K} \tag{2}$$

where $N = mg$, μ is the coefficient of kinetic friction, X_{n+1}, Xn are the vibration amplitudes at $n + 1$ and n sampling times, respectively, being $t_{n+1} - t_n = \frac{2\pi}{w_n}$. Shortly, to briefly clarify how the nonlinear gross-slip friction term affects system behavior, Figure 3 shows the response to one unit under the not-null initial position condition.

Figure 3 also shows that Coulomb friction causes the existence of multiple equilibrium positions, which indeed occur. The equilibrium positions can be determined by enforcing static equilibrium in the x-direction. The solution is a region defined by

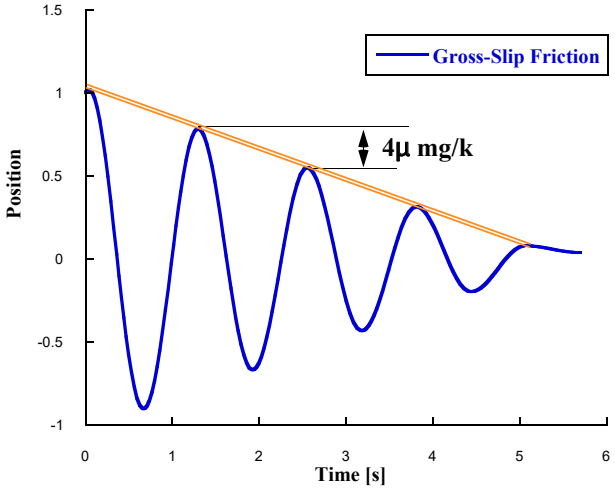

Figure 3. Response of the mass-spring system under gross-slip friction, without the derivative damper action, to a nonzero initial position. Conditions: $k = 5$ [N/m], $m = 0.20$ [Kg], $\mu = 0.15$.

$$\begin{matrix} \dot{x} = 0 \\ -\frac{\mu mg}{K} < x < \frac{\mu mg}{K} \end{matrix} \quad (3)$$

Depending on the initial conditions, the response will settle at a value x_e somewhere within this equilibrium region. Moreover, if the mass is subjected to an initial displacement within this equilibrium region, it will remain stationary as long as the initial velocity is zero. In short, Equation (3) reveals that increasing the proportional gain of the system will decrease the final error.

1.3. Rolling Friction: Brief Review

The effects of rolling friction were described in detail by Johnson (1985) [10], and only the more salient points are considered here. From a kinematics viewpoint, *rolling* is the relative angular velocity between two bodies about an axis lying in the tangent plane. Following Jhonson (1985), we define *free rolling* as a rolling motion in which the tangential force **f** is zero and *tractive rolling* as a rolling motion in which the tangential force **f** is nonzero but less than the limiting value:

$$f < \mu N$$

at which gross sliding occurs, and the direction of **f** is directly opposed to the direction of such gross sliding. Regarding the *tractive rolling* case, actually, the interfacial forces lead to a contact area of finite size, as shown in Figure 4; thus, the distribution of forces over this area can, therefore, lead to the transmission of a moment across the interface. In mechanical rolling contact situations, there is resistance to rolling, although its magnitude becomes much smaller than the resistance to sliding. Thus, considering an elastic rolling contact between the cylinder freely rolling on the trolley of our reference model under a normal load P per unit length in the axial direction of the cylinder, as illustrated in Figure 4, the local pressure, p, in the contact zone and the contact semiwidth, a, are known from the Hertz Equations [11,12].

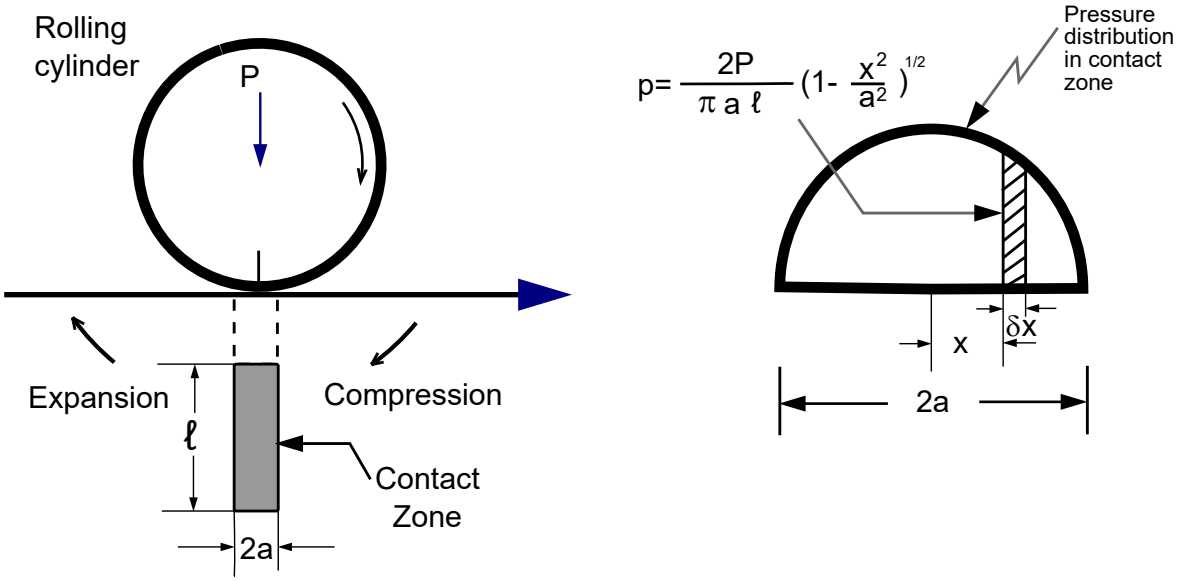

Figure 4. Elastic rolling contact of a cylinder rolling freely on a plane under normal load P.

Considering the striped strip in Figure 4 of width dx at point x, we can see that during forward compression of the contacting material, the normal force per unit length of the roller will be $p{\cdot}dx$, and this will exert a resistive moment about the center of the contact zone whose magnitude is $px\,dx$. Thus, the total moment exerted by all the elements on the front half of the roller cylinder will be

$$M = \int_0^a px\,dx = \int_0^a \frac{2P}{\pi a l}\left(1 - \frac{x^2}{a^2}\right)^{\frac{1}{2}} x dx = \frac{2Pa}{3\pi} \tag{4}$$

If the cylinder rolls forward through a distance x, the elastic work performed by this couple is given by

$$W = M\frac{x}{R} = \frac{2Pax}{3\pi R} \tag{5}$$

Under ideal conditions, the cylinder would be subjected to an equal and opposite moment arising from the pressure distribution in the rear half of the contact. However, owing to elastic hysteresis losses, not all the work is recovered and there is some dissipation energy. If we define the hysteresis loss by a coefficient ϵ, then the energy dissipated in rolling a distance x will be $\epsilon\, W$ and if this loss represents the rolling resistance, it follows that

$$F\,x = \epsilon\, W = \epsilon\,\frac{2Pax}{3\,\pi\,R} \tag{6}$$

where F is the force required to overcome the resistance. By analogy with sliding friction, the ratio $\frac{F}{P}$ can be defined as the coefficient of rolling resistance, λ, where

$$\lambda = \frac{2\epsilon\, a}{2\pi\, R} \tag{7}$$

Nonetheless, it is important to differentiate between losses in elastic contacts as the just studied case and losses in the presence of plastic deformations. Thus, rolling resistance in other cases arises from deformation-related losses. When considering deformation-related losses in a primary analysis, subsurface plastic deformation occurs only when the contact pressure on first contact exceeds a certain threshold value. If this is the case, the energy dissipated in such deformation can be considerably higher than that of the aforementioned case due to elastic hysteresis. However, owing to the accumulation of stress cycles during

rolling, the degree of plastic deformation reduces with cycling; thus, after a relative number of cycles, the deformation becomes fully elastic. This process is referred to as *shakedown* [13]. For this reason, this work assumes that load do not exceeds the *shakedown* limit stress, and thus, the present study is limited to the free rolling of an elastic cylinder on a perfectly elastic contact. Regarding the overall Figure 5, it reinforces the notion that under the elastic contact conditions, the response of the trolley–cylinder system remains undamped provided that hysteresis losses are considered negligibly small. Figure 5b depicts the impulse response of the roller, highlighting the nearly undamped x-position of its mass center. The response was obtained using Simscape Multibody Matlab Toolbox to numerically integrate the equations of motion for this single-benchmark mechanical system. Although this model may seem somewhat theoretical, there are numerous real-world systems that exhibit similar behavior:

- **1. Steel coil transport in manufacturing plants:** In the steel industry, steel coils (large rolls of metal sheets) are transported on trolleys within warehouses and production lines. These coils are often secured using elastic bands or flexible restraints to absorb vibrations during motion. If the trolley operates under proportional control to regulate its position or velocity, the resulting dynamics closely resemble those described in this study.
- **2. Pipe-laying systems for offshore installations:** In offshore platforms and specialized vessels, pipelines are deployed from a moving trolley or support structure, held by a tension-controlled system (such as elastic cables). The pipe rotates as it advances while the system compensates for external forces (marine currents, weight, etc.). Proportional control is applied to regulate the cable tension and the trolley's movement, making it a relevant analogy to the model studied.
- **3. Load transport in trucks or trains:** In some transportation applications, cylindrical objects (such as gas tanks, barrels, or cable reels) are secured with elastic straps** in trucks or railcars that move under automated control systems. When the vehicle accelerates or brakes, the load experiences oscillations similar to those described in the dynamic model. Figure 6 illustrates the first case.

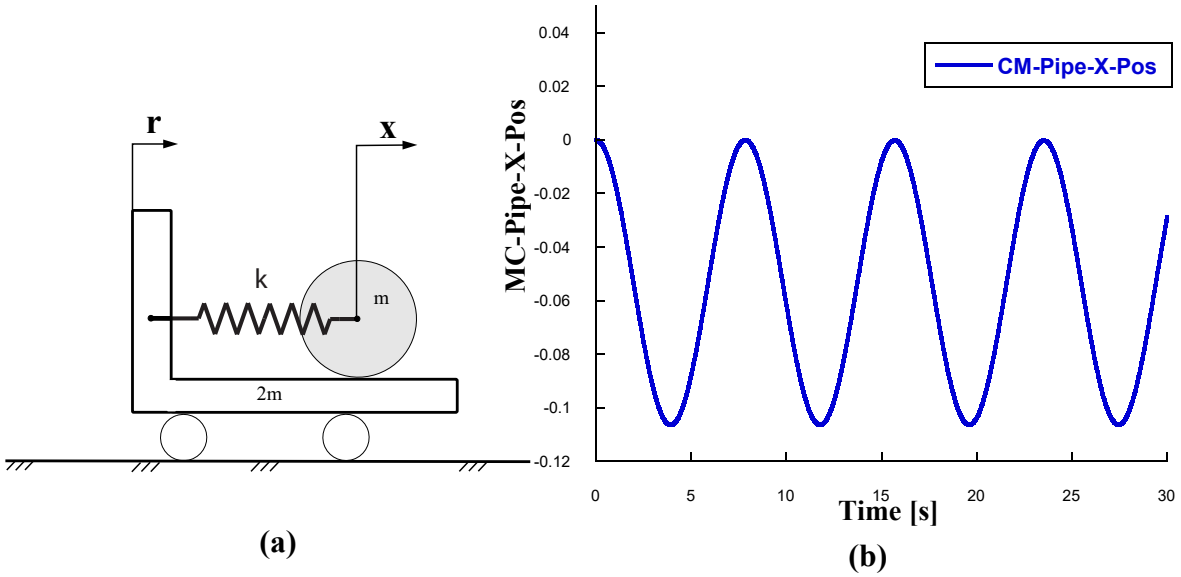

Figure 5. (**a**) Reference model of a two-mass and spring system undergoing rolling friction. (**b**) Impulse response of the rolling disc, showing the nearly undamped x-position of the mass center.

These examples illustrate practical cases where the dynamics of a trolley carrying a rolling cylindrical body, connected via an elastic element and controlled proportionally, are

observed in real-world engineering applications. Figure 6 illustrates the first real-world system case.



Figure 6. Steel coil transport system in manufacturing plants.

2. Materials and Methods

In any customary Input Shaping problem, the first step in addressing the design of an Input Shaping filter is to develop a simplified and affordable model of the system that allows for the estimation of its natural frequencies. In the actual system model, the pipe is modeled as a rolling disc attached to the trolley by a spring at its center of mass, while the trolley itself is connected to a guiding body frame by an additional spring acting as a proportional control. Lumped together, they form a Multibody Rigid-Plus-Flexible System (MRFS). In this work, dynamic analysis is carried out using two different approaches: the transfer matrix method and multibody techniques using the Simscape Multibody Toolbox available in Matlab-Mathworks, as previously mentioned. These two approaches are employed to cross-validate the results and ensure their consistency. The natural frequency values extracted from both models match, as demonstrated in the following.

2.1. Estimation of System Natural Frequencies Using the Transfer Matrix Method

The transfer matrix method was developed in the twentieth century to solve elasto-mechanical problems prior to the appearance of powerful computing facilities, such as Multibody. The matrix notation supports the modeling and analysis of mechanical systems with elastic elements, taking care of the various boundary conditions and initial conditions within the system and with respect to its environment [14]. The procedure to compute the vibration characteristics of our Multibody Rigid-Plus-Flexible System (MRFS) using the transfer matrix method (TMM) can be summarized as follows:

- Partition the dynamics model of the multibody system in a number of elements, as shown in Figure 7.
- Define the state vectors of the system in modal coordinates $Z_{i+1,i} = [X_{i+1,i}, Q_{i+1,i}]$.
- Write out the transfer matrix of each element.
- Assemble the overall transfer matrix and overall transfer equation.
- Form the characteristic equation according to boundary conditions.
- Obtain the natural frequencies by solving characteristic equation.
- Compute the eigenvectors and mode shapes.

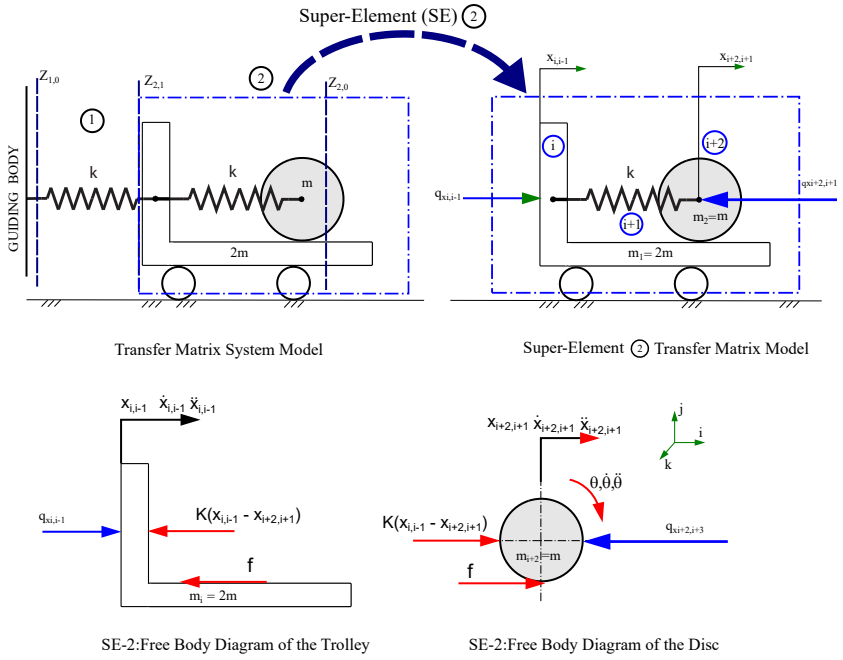

Figure 7. The Multibody System is broken up into the spring element ① and the super-element ②.

The conventions outlined in [14] are adopted below to develop this procedure. Thus, with reference to Figure 7, the transfer matrix system model is broken up into the spring element ① and the super-element (SE) ②; the latter is composed of the trolley cart plus the rolling cylinder as rigid bodies and the hinge spring K between them. The forces acting on the two bodies consist of the spring forces plus the friction force between the disc and the cart required to overcome the rolling resistance. In addition, a small negligible friction has been assumed between the cart and the reference frame. If this is the case, in the first step, the transfer matrix of the super-element formed by this trolley–spring–disc subset number as ② is estimated. The physical variables of position and force considered are detailed in Figure 7, where the modal coordinates $X_{i,i-1}$, $X_{i+2,i+1}$ denote the positions of the trolley and disc, respectively, and f represents the rolling friction force. Next, based on the free-body diagrams, the dynamic equations of each body within the super-element are formulated. The net force on the cart, equal to its mass times acceleration, is given by the equation

$$m_i \ddot{x}_{i,i-1} = q_{\mathrm{xi},i-1} - K(x_{i,i-1} - x_{i+2,i+1}) - f \tag{8}$$

Furthermore, considering the negative sign of torque due to the friction force f, the disc torque equation becomes

$$f \cdot R = \frac{1}{2} m_{i+2} \cdot R^2 \cdot \ddot{\theta}\left(-\hat{k}\right) \tag{9}$$

In addition, employing basic principles of kinematics,

$$\ddot{x}_{i+2,i+1} = \ddot{x}_{i,i-1} + R \cdot \ddot{\theta} \tag{10}$$

Solving for $\ddot{\theta}$ in (10) and substituting it into (9), the rolling friction force can be expressed as a function of the accelerations of the two bodies.

$$f = -\frac{1}{2} m_{i+2} \cdot (\ddot{x}_{i+2,i+1} - \ddot{x}_{i,i-1}\ ) \tag{11}$$

The net force on the rolling disc is equal to its mass times acceleration and is given by the equation

$$f + K(x_{i,i-1} - x_{i+2,i+1}) - q_{\mathrm{xi}+2,i+3} = m_{i+2} \cdot \ddot{x}_{i+2,i+1} \tag{12}$$

Furthermore, substituting (11) into (12) gives

$$-\frac{1}{2} m_{i+2} \cdot (\ddot{x}_{i+2,i+1} - \ddot{x}_{i,i-1}\ ) + K(x_{i,i-1} - x_{i+2,i+1}) - q_{\mathrm{xi}+2,i+3} = m_{i+2} \cdot \ddot{x}_{i+2,i+1} \tag{13}$$

We also substitute f from (11) into (20) to obtain

$$m_i \ddot{x}_{i,i-1} = q_{\mathrm{xi},i-1} - K(x_{i,i-1} - x_{i+2,i+1}) + \frac{1}{2} m_{i+2} \cdot (\ddot{x}_{i+2,i+1} - \ddot{x}_{i,i-1}\ ) \tag{14}$$

From (14), solving for $\ddot{x}i + 2, i + 1$ as a function of $xi, i - 1$ and $q_{\mathrm{xi},i-1}$, and applying algebraic manipulation, we obtain

$$-m_i \omega^2 X_{i,i-1} = q_{\mathrm{xi},i-1} - K(X_{i,i-1} - X_{i+2,i+1}) + \frac{1}{2} m_{i+2} \cdot \left(-\omega^2 X_{i+2,i+1} + \omega^2 X_{i,i-1}\ \right) \tag{15}$$

Now, transitioning to modal variables, we can express

$$-m_i \omega^2 X_{i,i-1} - \frac{1}{2} m_{i+2} \omega^2 X_{i,i-1} + K X_{i,i-1} - q_{\mathrm{xi},i-1} = K(X_{i+2,i+1}) + \frac{1}{2} m_{i+2} \cdot \left(-\omega^2 X_{i+2,i+1}\ \right) \tag{16}$$

Solving for $X_{i+2,i+1}$ we obtain

$$\left(K - \frac{1}{2} m_{i+2} \omega^2\right) X_{i+2,i+1} = K X_{i,i-1} - m_i \omega^2 X_{i,i-1} - \frac{1}{2} m_{i+2} \omega^2 X_{i,i-1} - q_{\mathrm{xi},i-1} \tag{17}$$

and arranging the terms as follows,

$$X_{i+2,i+1} = \frac{\left(K - \left(m_i + \frac{1}{2} m_{i+2}\right) \omega^2\right)}{\left(K - \frac{1}{2} m_{i+2} \omega^2\right)} X_{i,i-1} - \frac{1}{\left(K - \frac{1}{2} m_{i+2} \omega^2\right)} Q_{\mathrm{xi},i-1} \tag{18}$$

Now, starting from (13), which is restated here for clarity, we proceed to solve for $Q_{i+2,i+3}$

$$-\frac{1}{2} m_{i+2} \cdot (\ddot{x}_{i+2,i+1} - \ddot{x}_{i,i-1}\ ) + K(x_{i,i-1} - x_{i+2,i+1}) - m_{i+2} \cdot \ddot{x}_{i+2,i+1} = q_{\mathrm{xi}+2,i+3} \tag{19}$$

To this end, we revisit the trolley Equation (20)

$$m_i \ddot{x}_{i,i-1} = q_{\mathrm{xi},i-1} - K(x_{i,i-1} - x_{i+2,i+1}) - f \tag{20}$$

In Equation (20), we substitute the expression for f given in (11) as follows:

$$m_i \ddot{x}_{i,i-1} = q_{\mathrm{xi},i-1} - K(x_{i,i-1} - x_{i+2,i+1}) + \frac{1}{2} m_{i+2} \cdot (\ddot{x}_{i+2,i+1} - \ddot{x}_{i,i-1}\ ) \tag{21}$$

Rearranging the terms, we obtain

$$K(x_{i,i-1} - x_{i+2,i+1}) - \frac{1}{2} m_{i+2} \cdot (\ddot{x}_{i+2,i+1} - \ddot{x}_{i,i-1}\ ) = q_{\mathrm{xi},i-1} - m_i \ddot{x}_{i,i-1} \tag{22}$$

Now, the first term of this equation can be substituted into (13), yielding

$$q_{\mathrm{xi}+2,i+3} = q_{\mathrm{xi},i-1} - m_i \ddot{x}_{i,i-1} - m_{i+2} \cdot \ddot{x}_{i+2,i+1} \tag{23}$$

and again, transitioning to modal variables, we can write

$$Q_{\mathrm{xi}+2,i+3} = Q_{\mathrm{xi},i-1} + m_i\omega^2 X_{i,i-1} + m_{i+2}\omega^2 X_{i+2,i+1} \tag{24}$$

At this stage, it only remains to substitute the value of $X_{i+2,i+1}$, obtained in (18), to determine the value of the modal force variable $Q_{\mathrm{xi}+2,i+3}$ at the end-node of the super-element as a function of the modal variables at the first node. By substituting Equation (18) into Equation (24), we obtain

$$\begin{aligned} Q_{\mathrm{xi}+2,i+3} &= Q_{\mathrm{xi},i-1} + m_i\omega^2 X_{i,i-1} + \ldots \\ \ldots + m_{i+2}\cdot\omega^2 \cdot &\left[\frac{\left(K - \left(m_i + \frac{1}{2}m_{i+2}\right)\omega^2\right)}{\left(K - \frac{1}{2}m_{i+2}\omega^2\right)} X_{i,i-1} - \frac{1}{\left(K - \frac{1}{2}m_{i+2}\omega^2\right)} Q_{\mathrm{xi},i-1} \right] \end{aligned} \tag{25}$$

With some algebraic manipulation and the assistance of MATLAB's collect function, the equation can be simplified to

$$Q_{\mathrm{xi}+2,i+3} = \left[1 - \frac{m_{i+2}\omega^2}{\left(K - \frac{1}{2}m_{i+2}\omega^2\right)}\right] Q_{\mathrm{xi},i-1} + \left[m_i\omega^2 + m_{i+2}\omega^2 \cdot \frac{\left(K - \left(m_i + \frac{1}{2}m_{i+2}\right)\omega^2\right)}{\left(K - \frac{1}{2}m_{i+2}\omega^2\right)} \right] X_{i,i-1} \tag{26}$$

Then, using Equations (18) and (26) for $X_{i+2,i+1}$ and $Q_{i+2,i+3}$ expressed as functions of $X_{i,i-1}$ and $Q_{i,i-1}$, the super-element transfer matrix takes the form

$$\begin{bmatrix} X_{i+2,i+1} \\ Q_{\mathrm{xi}+2,i+3} \end{bmatrix} = \begin{bmatrix} \frac{\left(K - \left(m_i + \frac{1}{2}m_{i+2}\right)\omega^2\right)}{\left(K - \frac{1}{2}m_{i+2}\omega^2\right)} & -\frac{1}{\left(K - \frac{1}{2}m_{i+2}\omega^2\right)} \\ m_i\omega^2 + m_{i+2}\omega^2 \cdot \frac{\left(K - \left(m_i + \frac{1}{2}m_{i+2}\right)\omega^2\right)}{\left(K - \frac{m_{i+2}\omega^2}{2}\right)} & \left(1 - \frac{m_{i+2}\omega^2}{K - \frac{m_{i+2}\omega^2}{2}}\right) \end{bmatrix} \begin{bmatrix} X_{i,i-1} \\ Q_{\mathrm{xi},i-1} \end{bmatrix} \tag{27}$$

At this point, by substituting the corresponding mass values $m_i = 2m$ and $m_{i+2} = m$ into the generalized transfer matrix (27), the customized matrix is

$$U_2 = \begin{bmatrix} \frac{K - \frac{5}{2}m\omega^2}{K - \frac{1}{2}m\omega^2} & -\frac{1}{K - \frac{1}{2}m\omega^2} \\ 2m\omega^2 + \frac{m\omega^2\left(K - \frac{5}{2}m\omega^2\right)}{K - \frac{1}{2}m\omega^2} & 1 - \frac{m\omega^2}{K - \frac{1}{2}m\omega^2} \end{bmatrix} \tag{28}$$

The dynamics of the MRFS depend directly on physical parameters, meaning that changes in values such as the disc mass m affect the system's natural frequencies. Since these frequency variations stem from parameter changes, analytically estimating their dependence offers advantages in designing the Input Shaping Filter to adapt to frequency shifts. For the transfer matrix model of the MRFS (Figure 7), natural frequencies are estimated in two steps. First, the state vector at $Z_{2,0}$ is related to the modal state variables at $Z_{1,0}$ by multiplying the transfer matrices of the super-element ② and the spring element ①, which acts as proportional control, as follows:

$$\begin{aligned} Z_{2,0} &= U_2 U_1 Z_{1,0} \\ \begin{bmatrix} X_{2,0} \\ Q_{2,0} \end{bmatrix} &= \begin{bmatrix} \frac{K - \frac{5}{2}m\omega^2}{K - \frac{1}{2}m\omega^2} & -\frac{1}{K - \frac{1}{2}m\omega^2} \\ 2m\omega^2 + \frac{m\omega^2\left(K - \frac{5}{2}m\omega^2\right)}{K - \frac{1}{2}m\omega^2} & 1 - \frac{m\omega^2}{K - \frac{1}{2}m\omega^2} \end{bmatrix} \begin{bmatrix} 1 & -1/K \\ 0 & 1 \end{bmatrix} \begin{bmatrix} X_{1,0} \\ Q_{1,0} \end{bmatrix} \end{aligned} \tag{29}$$

Then, the boundary conditions determine the value of the state vector $Z_{2,0}$ at the end of the chain: $X_{2,0} \neq 0$ plus $Q_{2,0}$= 0. We see that each row of the global matrix Equation (29) is an equation of force or displacement. The equations of force determine the frequency

characteristic equation, while the equations of displacement determine the mode shape. For the first case, the boundary conditions allow us to write

$$\begin{bmatrix} X_{2,0} \neq 0 \\ Q_{2,0} = 0 \end{bmatrix} = \underbrace{\begin{bmatrix} u_{1,1} & u_{1,2} \\ u_{2,1} & u_{2,2} \end{bmatrix}}_{U} \begin{bmatrix} X_{1,0} = 0 \\ Q_{1,0} \neq 0 \end{bmatrix} \tag{30}$$

The nontrivial solution of (30) requires that

$$u_{2,2} = 0 \tag{31}$$

From this point, symbolic MATLAB R2024 computation is used to obtain the natural frequencies as a function of physical parameters. Solving for w in (31) gives

$$\begin{pmatrix} -\sqrt{\frac{K}{m}} \\ -\frac{\sqrt{14}\sqrt{\frac{K}{m}}}{7} \\ \frac{\sqrt{14}\sqrt{\frac{K}{m}}}{7} \\ \sqrt{\frac{K}{m}} \end{pmatrix} \tag{32}$$

Thus, the system natural frequencies are

$$\begin{aligned} \omega_1 &= \sqrt{\lambda_1} = \sqrt{\frac{K}{m}} \\ \omega_2 &= \sqrt{\lambda_2} = \sqrt{\frac{2K}{7m}} \end{aligned} \tag{33}$$

Using these analytical expressions of natural frequencies and values of the parameters m = 1 [Kg], k_p = k = 1 [N/m], the numerical values explained in Table 1 are obtained.

Table 1. System natural frequencies' analytical expressions and corresponding numerical values.

ω Expression $\frac{\text{rad}}{\text{s}}$	Numerical Value $\frac{\text{rad}}{\text{s}}$	Numerical Frequency [Hz]
$\omega_1 = \sqrt{\frac{K}{m}}$	$\sqrt{1}$	$f_1 = \frac{\omega_1}{2\pi} = 0.1592$
$\omega_2 = \sqrt{\frac{2K}{7m}}$	$\sqrt{\frac{2}{7}} = 0.5345$	$f_2 = \frac{\omega_2}{2\pi} = 0.0851$

2.2. The Multibody System Model

To verify that the above dynamic analysis and the values corresponding to these natural frequencies are correct, a systematic treatment of the dynamic behavior of the interconnected bodies led to a multibody model of the system setup by means of a prismatic or translational kinematic joint between the carriage and the reference frame, treating the rolling contact between the pipe and the trolley; a six-DOF joint was chosen from Matlab's Simscape-Multibody kinematic joint library. The two springs were also placed between the frame and the rear face of the trolley and the front face of the trolley, taking into account the center of mass of the pipe, although the established elastic forces are not visible in the Matlab Simscape Mechanical Explorer shown in Figure 8. The rolling contact between the pipe and the trolley was modeled using a smooth spring-damper approach, with stiffness and damping parameters detailed in Tables 2 and 3. This approach ensures numerical stability while capturing the essential dynamics of rolling friction.

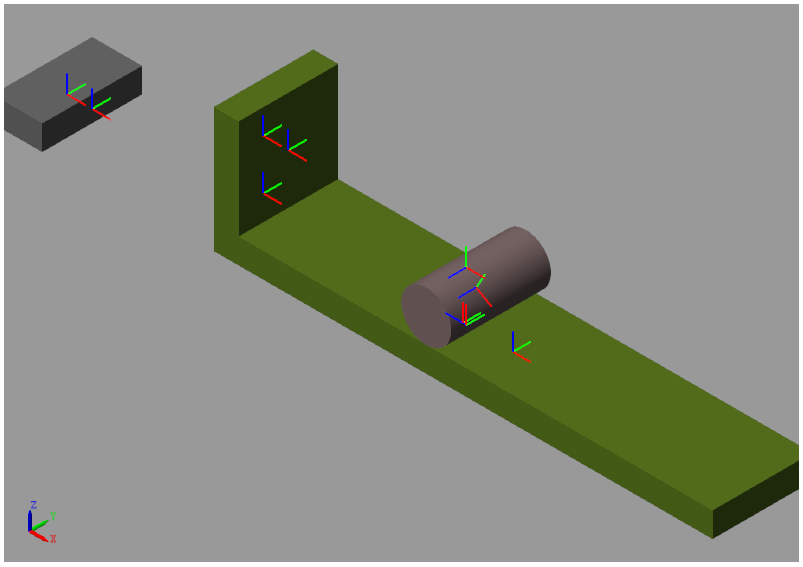

Figure 8. Simscape Mechanical Explorer Sketch of the system showing the body frames.

Table 2. Normal force customized parameters.

Method [1] Transition Region With	Stiffness	Damping
Smooth spring damper	1×10^6 N/m	1×10^3 N/(m/s)

[1] Transition region with 1×10^{-4} m.

Table 3. Friction force customized parameters.

Method [1]	Coefficient of Static Friction	Coefficient of Dynamic Friction
Smooth stick slip	0.3	0.3

[1] Critical velocity 1 [m/s].

Given the inherent complexity of rolling the pipe on the trolley, the multibody model shown in Figure 9 has not been imported from any CAD before; on the contrary, it has been built by customizing the objects corresponding to the bodies, kinematic joints, and frame transforms, which have been imported directly from the Simscape Multibody toolbox along with a manual interconnection between them. About the inertial properties of bodies, the trolley has been modeled as a concentrated mass point at is mass center, in other words, as a Newton model, while the pipe has distributed mass with not-null moments of inertia plus products of inertia.

A small initial impact of the tube on the surface of the trolley causes the mechanical vibration of this flexible system. Then, logging the signal corresponding to the abscissa position of the center of mass of the pipe allows experimentally measuring the system natural frequencies by carrying out a FFT on this signal. As demonstrated in Figure 10, the low-frequency component of the logged signal value is $f_2 = 0.07998$, while the high-frequency component value is $f_1 = 0.159997$. Both values, extracted from the multibody model simulation, coincide with the analytical values depicted in Table 1. This reinforces the notion that both the flexible system dynamic analysis plus the system's multibody model are correct.

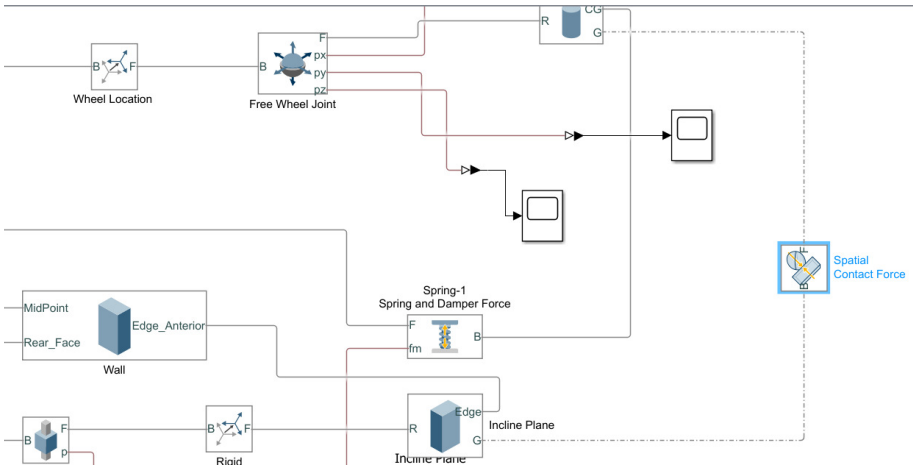

Figure 9. Simscape (Matlab) multibody model of the system showing bodies interconnected by kinematics joints plus a large number of important multibody formalisms by rigid frame transforms plus body and joint customizations.

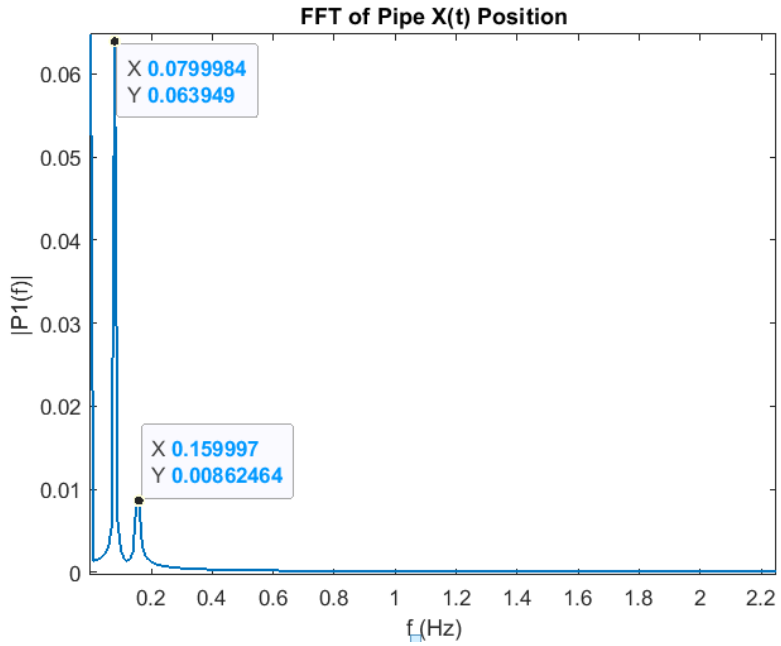

Figure 10. FFT of the signal corresponding to the abscissa position of the center of mass of the pipe. Low-frequency component value 0.079998 [Hz]. High-frequency component 0.159997 [Hz].

2.3. Convolved–ZVD-ZVD Shaper

Note that the ratio between the two natural frequencies of this two-mode undamped system becomes $\frac{f_1}{f_2} = \frac{0.159997}{0.07998} = 2.0005$. Input scavenging filters for undamped systems, as in this case, have the property of canceling vibration at the modeled frequency and at odd multiples of it. Given this frequency ratio, in this case, this property is not useful to us, and the most appealing solution consists of using a convolved shaper resulting from the convolution sum between two ZVD filters for each of the single-mode frequencies, as follows:

$$ZVD_{f_1=0.159997} = \begin{bmatrix} A_i \\ T_i \end{bmatrix} = \begin{bmatrix} 0.3344 & 0.4877 & 0.1778 \\ 0 & 3.1408 & 6.2816 \end{bmatrix} \tag{34}$$

$$ZVD_{f_2=0.07998} = \begin{bmatrix} A_i \\ T_i \end{bmatrix} = \begin{bmatrix} 0.3344 & 0.4877 & 0.1778 \\ 0 & 6.2831 & 12.5661 \end{bmatrix} \tag{35}$$

At this point, by carrying out the convolution sum between these two ZVD shapers, a time delay filter (TDF) is obtained that attenuates the amplitude of the vibration at both frequencies given by

$$ZVD_{f_1,f_2} = \begin{bmatrix} A_i \\ T_i \end{bmatrix} = \begin{bmatrix} 0.1118 & 0.1631 & 0.0595 & 0.1631 & 0.2379 & 0.0887 & 0.0595 & 0.0867 & 0.0316 \\ 0 & 3.140 & 6.281 & 6.281 & 9.422 & 12.563 & 12.565 & 15.705 & 18.846 \end{bmatrix} \quad (36)$$

The convolved two-mode ZVD-ZVD shaper was designed to address the natural frequencies, as defined in Equation (33). By combining two ZVD filters, this shaper attenuates vibrations at both frequencies while maintaining robustness to parameter uncertainties, as illustrated in the sensitivity curves of Figure 11. This two-mode ZVD-ZVD shaper has nine filter taps; the delay induced by it increases by 6 s when compared to the ZVD filter at the lowest frequency f_2. The corresponding sensitivity curves for the single-mode shapers and the convolved two-mode shaper are shown in Figure 11. The convolved shaper is very robust to modeling errors of the 0.07998 Hz mode. Furthermore, the second mode can range from between 0.11 Hz and 0.20 Hz, and the residual vibration will remain small, significantly below a tolerable level V_{tol}: 10%. Note that the suppression of the convolved shaper near 0.24 Hz is due to the contribution from the 0.07998 Hz shaper. This is because single-mode shapers suppress vibration at odd multiples of their designed undamped frequency. Thus, when an input shaper is convolved with a second shaper, the vibration suppression properties at these higher frequencies are passed on to the resulting two-mode shaper.

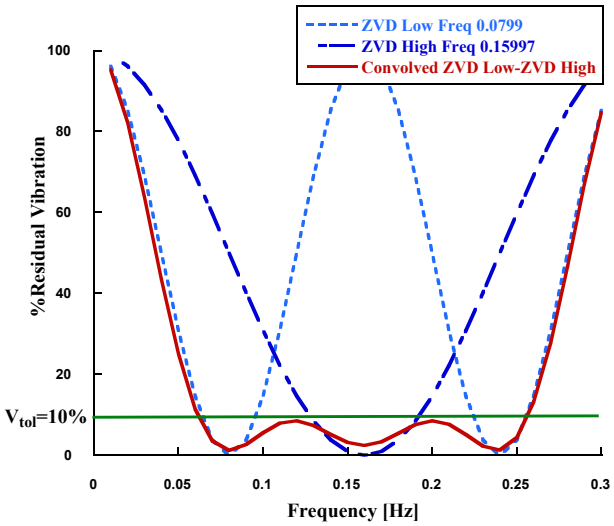

Figure 11. Convolved two-mode ZVD-ZVD shaper for f_1: 0.07998 and f_2: 0.159997 Hz undamped frequencies.

2.4. Two-Mode Direct Input Shaper Design by Simultaneous Constraints

The convolved two-mode ZVD-ZVD shaper has a length of

$$\begin{aligned} T_9 &= T_{\omega_1} + T_{\omega_2} \\ T_9 &= 6.28 + 12.56 = 18.846[s] \end{aligned} \quad (37)$$

Thus, the induced delay consists of the sum of the duration corresponding to the single-mode shapers. This is a drawback.

Nonetheless, unlike the convolved shaper, where the constraints on each mode are solved independently, the constraints equations for both modes can be solved jointly with the help of an optimization software program. If this is the case, the most appealing options are the General Algebraic Modeling Systems (GAMS) and the Matlab Optimization Toolbox.

The outcomes of the optimization problem are two-mode shapers that are shorter than the convolved shaper. To be specific, if the mode ratio $R = \frac{\omega_1}{\omega_2}$ is up to three, then the optimized ZVD-ZVD shaper only has five impulses as per Rappole [15]. However since the closed-form solutions proposed by Rappole are difficult to obtain analytically, we obtain a multimode input shaper by listing all the constraint equations for each mode and solving them numerically and simultaneously. As stated before, the advantage of this two-mode input shaper, compared to one obtained by convolution, is that it has fewer impulses and generally a shorter duration [16]. Note that the process of obtaining it is more difficult. The two-mode input shaper derived here from this method relies on the numerical solutions of the following optimization problem.

$$min\, T_5 \tag{38}$$

subject to the constraint equations

$$\begin{gathered}
\sum_i^N A_i e^{\zeta\omega_1 t_i} cos(\omega_{d1} t_i) = 0, \sum_i^N A_i e^{\zeta\omega_1 t_i} sin(\omega_{d1} t_i) = 0 \\
\sum_i^N A_i t_i e^{\zeta\omega_1 t_i} cos(\omega_{d1} t_i) = 0, \sum_i^N A_i t_i e^{\zeta\omega_1 t_i} sin(\omega_{d1} t_i) = 0 \\
\sum_i^N A_i e^{\zeta\omega_2 t_i} cos(\omega_{d2} t_i) = 0, \sum_i^N A_i e^{\zeta\omega_2 t_i} sin(\omega_{d2} t_i) = 0 \\
\sum_i^N A_i t_i e^{\zeta\omega_2 t_i} cos(\omega_{d2} t_i) = 0, \sum_i^N A_i t_i e^{\zeta\omega_2 t_i} sin(\omega_{d2} t_i) = 0 \\
\sum_i^N A_i = 1, t_1 = 0
\end{gathered} \tag{39}$$

Since Equation (39) consists of ten equations, a solution can be determined when there are ten unknowns. Denoting the ten unknowns as $A_1, A_2, A_3, A_4, A_5, T_1, T_2, T_3, T_4, T_5$, the input shaper will consist of five impulses. Thus, from Equation (39), N = 5. Assuming N = 5 and solving for the objective Equation (38), subject to the constraints of Equation (39), numerically with the help of the Matlab Optimization Toolbox, we obtain the following two-mode input shaper for $w_1 = 2\pi 0.15997$, $w_2 = 2\pi 0.07998$ and $\zeta_1 = \zeta_2 = 0.0$.

$$ZVD - ZVD_{f_1,f_2} = \begin{bmatrix} A_i \\ T_i \end{bmatrix} = \begin{bmatrix} 0.1112 & 0.2222 & 0.3333 & 0.2222 & 0.1112 \\ 0 & 4.1671 & 8.3341 & 12.5012 & 16.6683 \end{bmatrix} \tag{40}$$

Regarding the sensitivity curve corresponding to this shaper shown in Figure 12, one can appreciate that it is less robust than the convolved shaper. That is, the frequency range under which the % residual vibration remains below 10% is lower than in the case of the aforementioned convolved shaper. In the Input Shaping design pursuit to reduce the shaper-induced delay, it is common for robustness to be sacrificed. Table 4 shows the comparative robustness analysis of both the convolved and the direct shapers, which reinforces the previous statement. Note that in the case of the direct shaper, a damping ratio value $\zeta_{1,2}$:0.0 was also assumed.

Table 4. Convolved and direct two-mode **robustness**.

Two-Mode Shaper	Frequency Range	Width and Percentage %
Convolved	[0.05 0.25] Hz	0.20 Hz—100%
Direct [1]	[0.0611 0.1786] Hz	0.1175 Hz—58.75%

[1] Simultaneous constraints.

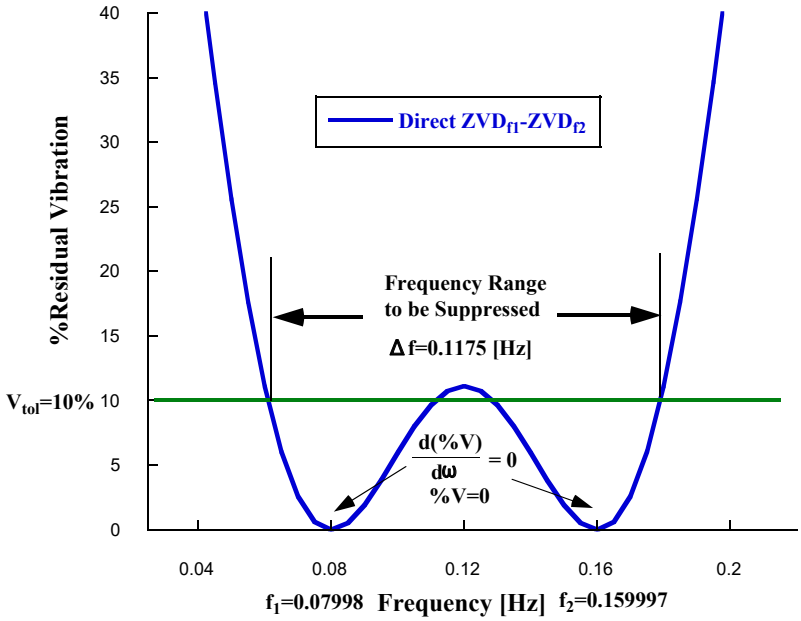

Figure 12. Two-mode input shaper by simultaneous constraints for f_1 : 0.07998 and f_2 : 0.159997 [Hz] and ζ: 0.0.

3. Results

Experimental simulations were performed on the multibody model of the pipe transport system introduced in Section 2.3. The input motion is fed to the prismatic joint between the guide body with high inertia, in gray in Figure 8, and the frame of reference. The corresponding Z-prismatic primitive joint **Pz** is customized as follows (Table 5).

Table 5. Z Prismatic primitive joint **actuation**.

Force	Motion
Automatically computed Follower on base	Provided by input Resolution frame base [1]

[1] Mode configuration: normal.

This translational prismatic joint was subjected to two different motion input profiles, the first of which is shown in Figure 13. It is a trapezoidal profile where the ramp-up phase lasts for 17 s. This duration aligns with the time delay corresponding to the direct shaper, which was previously calculated in the preceding section as 16.6683 s. It is essential for the ramp-up duration to be equal to or greater than the time delay filter's duration to ensure that the convolution operation with the filter's coefficients produces a well-suited smooth signal.

The multibody model's response for the pipe transport system is selected as the position along the X-axis of the pipe's center of mass, modeled as a cylinder. Figure 14 shows the dynamic responses to this trapezoidal motion, both when the signal is unfiltered and when it is filtered using the two-mode direct shaper under simultaneous constraints. It must be acknowledged that these initial results are encouraging. The results presented in Table 6 highlight the benefits of using the direct–ZVD-ZVD shaped input motion compared to the unshaped input motion in reducing vibration amplitudes in the trolley–pipe system. However, the findings also emphasize that residual vibrations are not entirely eliminated. Key observations include the following:

- **Reduction in maximum and minimum response values**. The use of the direct–ZVD-ZVD shaped input motion achieved a 14.95% reduction in overshoot compared to the

unshaped input, with peak amplitudes decreasing from 2.376 to 2.02. This improvement reflects the shaping filter's ability to mitigate excessive oscillations effectively.

- **Improvement in median values**. Its median value (0.3289) is closer to the center of the distribution than the unshaped case (0.3173), suggesting a more stable and predictable system behavior.
- **Reduction in mode and standard deviation**: The mode of the shaped input (-0.01324) clearly shows a more balanced response compared to the unshaped input (-0.1686). Nonetheless,the standard deviation values—0.6573 (unshaped) and 0.6174 (shaped)—indicate a marginal improvement in the uniformity of the shaped response.

In short, the direct–ZVD-ZVD shaping technique demonstrates clear promising benefits in controlling the trolley–pipe system by reducing extreme oscillations, improving stability, and minimizing response variability. These modest results, which can be observed in Figure 14 and Table 6, underline the effectiveness of Input Shaping in mitigating undesired dynamic effects and enhancing system performance. Nonetheless, while the shaped input motion improves the system's performance, further refinements dealing with rolling friction compensation in order to linearize the system might be necessary to achieve a more meaningful attenuation of residual vibration at the move end.

Table 6. Comparison of unshaped and Direct–ZVD-ZVD responses. The ramp-up lasts for 17 [s] .

Input [1]	Min	Max	Median	Mode	Std
Unshaped	-0.1686	2.376	0.3173	-0.1686	0.6573
Direct–ZVD-ZVD	-0.01324	2.02	0.3289	-0.01324	0.6174

[1] Units in meters [m].

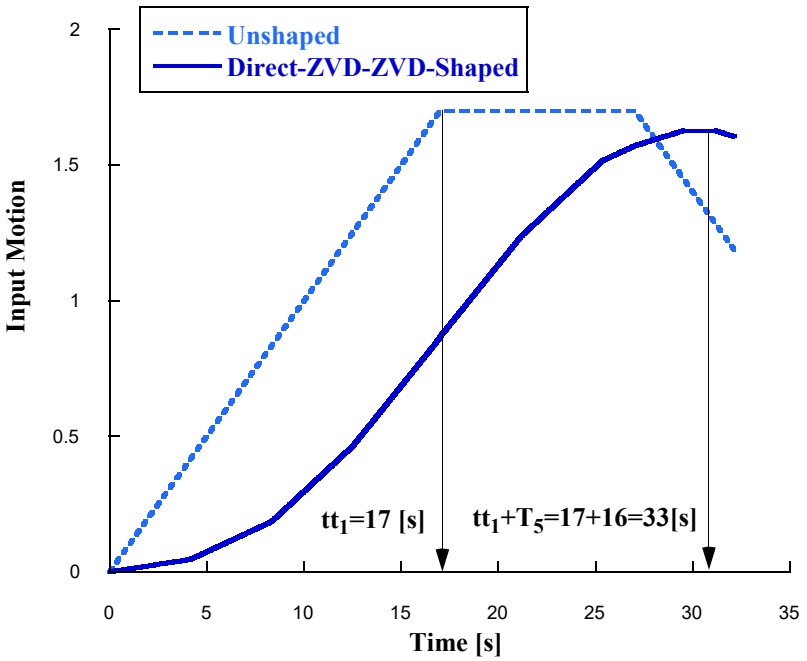

Figure 13. Trapezoidal input motion. Conditions: the ramp-up lasts for tt_1: 17 [s]. Unshaped input motion. Direct–ZVD-ZVD shaped input motion. Conditions: ramp-up lasts for $tt_1 + T_5$: 33 [s].

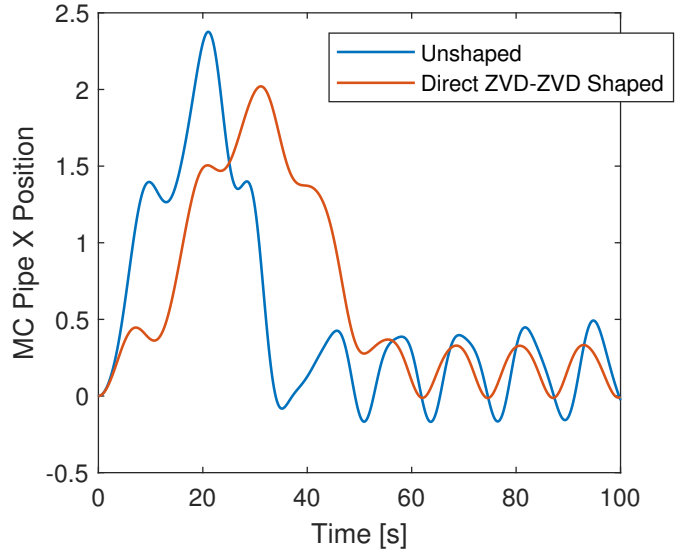

Figure 14. Multibody model pipe mass center X-position responses to trapezoidal input motion profile with 12 s ramp-up. Pipe mass center X-position unshaped response. Pipe mass center X-position shaped response for direct–ZVD-ZVD shaped input motion.

In view of this, dynamic simulations for the convolved shaper were also conducted and are shown in Figures 15 and 16. Regarding Figure 15, note that in this case, the ramp-up lasts for tt_1: 20 [s], almost two seconds longer than the time duration of the convolved two-mode ZVD-ZVD time delay filter whose last impulse occurs at T_9: 18.846 [s]. Thus, the convolved–ZVD-ZVD shaped input motion ramp-up lasts for 38.846 [s], as shown in Figure 15. The shaper duration is important because it limits the system rise time; an increase in shaper length degrades system rise time.

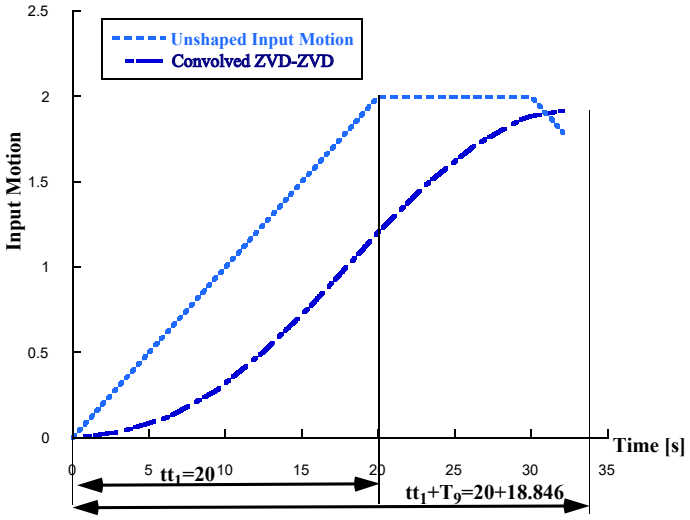

Figure 15. Trapezoidal input motion. Conditions: the ramp-up lasts for tt_1: 20 [s]. Unshaped input motion. Convolved–ZVD-ZVD shaped input motion.

Nonetheless, the convolved two-mode ZVD-ZVD shaper does improve the dynamic response of the trolley–pipe benchmark transport system. The following points are demonstrated in Figure 16 and Table 7:

- **Observations on peak amplitude reduction**. The convolved–ZVD-ZVD shaped input significantly reduces the peak amplitude compared to the unshaped input. Specifically, the maximum value decreases from 2.651 to 2.297, representing a 13.36% reduction in

overshoot. This demonstrates the convolved shaping filter's effectiveness in mitigating extreme oscillations.

- **Improved stability and reduced variability**. The standard deviation (std) decreases from 1.024 (unshaped) to 0.7322 (shaped), highlighting a notable improvement in response uniformity. The median shifts from a negative value (−0.3299) to a positive one (0.4213), indicating a change in the response distribution, likely due to the smoother dynamics introduced by the shaping process.
- **Limitations: residual vibration.** Despite the improvements, residual vibrations persist: the minimum value improves only slightly, from −0.8821 to −0.0033, showing that while oscillations are dampened, complete cancellation is not achieved.

Again, as in the direct shaper case, residual vibration at move end persists, along with deviations, after the time that the last impulse is applied, reflecting that the shaped response still requires further optimization by linearizing the system using rolling friction compensation, especially for systems requiring high precision.

Table 7. Comparison of unshaped and convolved–ZVD-ZVD responses. Ramp-up lasts for 20 [s].

Input [1]	Min	Max	Median	Mode	Std
Unshaped	−0.8821	2.651	−0.3299	−0.8821	1.024
Convolved–ZVD-ZVD shaped	−0.0033	2.297	0.4213	−0.00333	0.7322

[1] Units in meters [m].

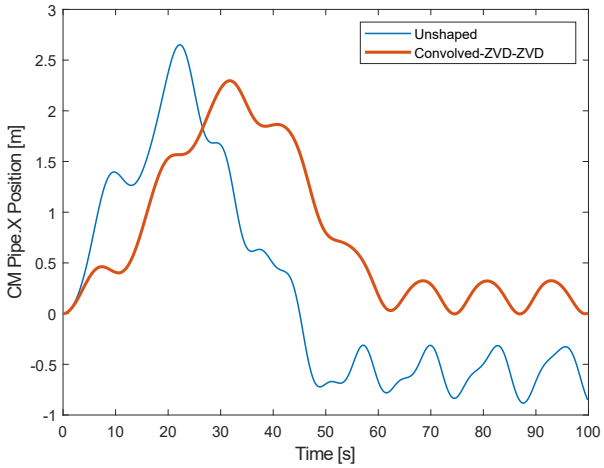

Figure 16. Experimental trapezoidal input motion profile responses. Pipe mass center X-position unshaped response. Pipe mass center X-position for convolved–ZVD-ZVD shaped response.

4. Discussion

4.1. Effectiveness Criterion for Input Shaping

The customary criterion used in Input Shaping studies to assess its effectiveness is the **percentage reduction in the amplitude of residual vibration** when comparing the response to the unshaped command and the response to the shaped command.

In our study, the input motion follows a *rest-to-rest trajectory* with a maximum displacement set point of 2 [m]. Under this condition, the direct–ZVD shaper reduces the peak-to-peak amplitude of the residual vibration from 0.6483 [m] (unshaped command) to 0.3418 [m], corresponding to a 47.3% reduction.

While purely linear systems can achieve higher reductions—up to 95%—the presence of rolling friction nonlinearities in our trolley–pipe benchmark system naturally limits the

achievable performance. Nevertheless, this moderate improvement, representing only 17.1% of the total displacement, highlights the robustness of the direct–ZVD shaper in mitigating unwanted oscillations even in nonlinear environments.

These primary results reinforce the notion of the practical applicability of Input Shaping in real-world transport mechanisms undergoing rolling friction, providing a promising strategy for vibration suppression even in the presence of rolling friction.

A detailed comparative analysis is developed below based on the direct–ZVD-ZVD and convolved–ZVD-ZVD responses depicted in Figures 14 and 16 plus the previous data given in Tables 6 and 7.

4.2. Detailed Comparative Analysis

Peak Amplitude Reduction

- DIRECT–ZVD-ZVD: The maximum amplitude is 2.02, compared to the unshaped value of 2.376, which represents a reduction in overshoot of around the 15%.
- CONVOLVED–ZVD-ZVD: The maximum amplitude is 2.297, compared to the unshaped value of 2.651, which represents a 13.36% reduction in overshoot.

Observation: Although both filters reduce the overshoot, the direct–ZVD-ZVD achieves slightly better performance in peak amplitude suppression.

Response Variability (Standard Deviation)

- DIRECT–ZVD-ZVD: The standard deviation is 0.6174, a reduction from the unshaped value of 0.6573.
- CONVOLVED–ZVD-ZVD: The standard deviation is 0.7322, compared to the unshaped value of 1.024.

Observation: The convolved–ZVD-ZVD achieves a more noticeable reduction in response variability, indicating smoother system behavior overall, but the absolute values of variability remain slightly higher than the Direct–ZVD-ZVD.

Residual Vibrations

- DIRECT–ZVD-ZVD: The minimum value is -0.01324, indicating very small oscillations below the baseline.
- CONVOLVED–ZVD-ZVD: The minimum value is -0.0033, which also represents a low level of oscillation.

Observation: Both methods effectively suppress negative oscillations, but the convolved–ZVD-ZVD slightly outperforms the direct method in minimizing residual vibrations.

Central Tendency (Median and Mode)

- DIRECT–ZVD-ZVD: The median is 0.3289, and the mode is -0.01324.
- CONVOLVED–ZVD-ZVD: The median is 0.4213, and the mode is -0.00333.

Observation: The convolved–ZVD-ZVD has a higher median value, suggesting a better balance in the response distribution. Its mode also shows minimal oscillations compared to the direct method.

Key Takeaways

- PEAK SUPPRESSION: The Direct–ZVD-ZVD achieves slightly better peak suppression, with a higher percentage reduction in maximum amplitude.
- SMOOTHNESS AND VARIABILITY: The convolved-VD-ZVD excels at reducing overall variability, providing a smoother response over time.
- RESIDUAL VIBRATIONS: Both methods perform well, but the convolved–ZVD-ZVD has a slight edge in minimizing residual oscillations.

Based on Hekman et al. [17], the performance of the Input Shaping without Coulomb friction compensation should degrade as the input motion size decreases. The results that

have just been obtained for the rolling friction case somewhat reinforce this theory. In this work, no explicit compensation was used for the friction that allows rolling. Without such explicit compensation for rolling friction, the results of Input Shaping worsen when the duration of the motion command is reduced, as in the case of the direct shaper, while when the duration of input motion is increased for the convolved shaper case, the dynamic response of the system to the shaped input motion improves for the corresponding unshaped and direct shaped cases. The drawback of cancelling multiple frequencies is that the duration of the convolved shaper increases rapidly and, consequently, so does the overall rise time of the system.

5. Conclusions and Future Research

Conclusions

In this work, the performances of Input Shaping without rolling friction compensation for a trolley–pipe benchmark transport system were studied. As in any Input Shaping problem, the natural frequencies of this benchmark mechanical system were first estimated analytically. To this end, the Newton–Euler laws that govern its dynamics were proposed and the differential equations that describe it were obtained. Thus, modal variables were used and the associated eigenvalue problem was solved by obtaining the natural frequencies in symbolic notation. By customizing the values of the inertial and elasticity parameters of the system, the corresponding numerical values of these theoretical frequencies were obtained. At this point, first, in order to validate these frequencies, a multibody model of the system was built in the Matlab Simulink-Simscape-Multibody environment, and we customized it with the same values of the inertial and elastic parameters. Logging the signal of the cylinder's mass center x-position, the FFT of this signal was carried out, obtaining the same values for the frequency components as those estimated analytically, this time by experimental simulation of the multibody model.

Although it was possible to accurately and reliably estimate the vibration frequencies of the system, unlike in other works such as [18], and to employ robust two-mode input shapers, namely, the simultaneous-constraints direct shaper and the convolved ZVD_{low}-ZVD_{high} shaper, only modest positive results were achieved in terms of improving the dynamic response. Specifically, these improvements included a reduction in overshoot, a decrease in residual vibration amplitude at the end of the motion, and enhanced positioning accuracy at the final set point.

In any case, the system's nonlinearity creates a significant challenge for conventional Input Shaping strategies. This nonlinearity arises from the reversal of the rolling frictional force, which does not remain constant. Unlike the gross-slip scenario studied in previous works [17–19], the frictional force depends on the accelerations of the trolley and the disc, as described by Equation (11). This dependency demonstrates that conventional Input Shaping methods alone are insufficient to address the complexities of this system.

Thus, a dynamic compensation approach, which linearizes the system, becomes paramount and remains still unanswered.

6. Future Research

While this study has demonstrated the effectiveness of Input Shaping in mitigating vibrations in rolling contact systems, some limitations remain due to the nonlinear effects introduced by rolling friction. One promising direction for future research is the development of an **adaptive dynamic model** that estimates and compensates for rolling resistance in real time.

Since rolling friction depends on the accelerations of both the trolley and the rolling disc, a **state observer** (e.g., Luenberger observer or Kalman filter) could be implemented

to dynamically estimate this force based on acceleration measurements. Once estimated, a **compensation force** F_c can be applied in the dynamic equations to counteract rolling friction and further linearize the system response.

While both a Luenberger Observer and a Kalman Filter were considered for future compensation of rolling friction to further linearize the system, the Luenberger Observer appears to be the more suitable option. This is due to its simpler implementation and faster response time, which minimizes additional delays that could otherwise accumulate alongside the inherent delay of Input Shaping. Although the Kalman Filter offers optimal estimation under certain conditions, its computational complexity and potential to introduce further delays make the Luenberger Observer a more practical choice for real-time applications in vibration control.

Once the system is effectively linearized through rolling friction compensation using a **Luenberger Observer**, a subsequent step would involve **redesigning the Input Shaping filter** to optimize performance under the newly linearized conditions. By tailoring the Input Shaping strategy to the compensated system dynamics, it is possible to achieve more precise vibration suppression and further reduce residual oscillations. This iterative approach ensures that the control strategy remains robust, even as the system transitions from nonlinear to linear behavior, ultimately enhancing its effectiveness in real-world applications where rolling friction can vary with operational conditions.

Additionally, further validation through **experimental implementations** would be crucial to confirm the feasibility of these methods in practical applications. Future studies could focus on designing real-time controllers that adaptively adjust Input Shaping parameters in response to rolling friction variations.

By addressing these challenges, future work will contribute to a more comprehensive control framework for rolling-contact systems, enhancing the applicability of Input Shaping in nonlinear mechanical systems.

Such compensation is necessary for Input Shaping to fully deliver its benefits to the system's dynamics. Thus it will be addressed in the future research.

Author Contributions: G.P. (Gustavo Peláez) and P.I.: review and editing (equal); G.P. (Gerardo Peláez): writing—original draft (lead); H.R.: formal analysis (lead); G.P. (Gerardo Peláez): software (lead); G.P. (Gerardo Peláez): writing—review and editing (equal); H.R.: supervision and project administration; H.R.: funding acquisition. All authors have read and agreed to the published version of the manuscript.

Funding: This research was funded by the Spanish government's Ministry of Science and Innovation Grant Number PID2020-116984RB-C21.

Data Availability Statement: Suggested data availability statements are available at https://www.facebook.com/gerardo.pelaezlourido/videos/1092810542094036 (accessed on 7 February 2025).

Acknowledgments: We would like to thank William E. Singhose and Tarunraj Singh for their helpful perspectives and suggestions regarding how to solve Input Shaping optimization problems using the Matlab Optimization Toolbox software R2024.

Conflicts of Interest: The authors declare no conflicts of interest.

Abbreviations

The following abbreviations are used in this manuscript:

ZVD	Zero vibration shaper
TDF	Time delay filter
GAMS	General Algebraic Modeling Systems
FBD	Free-body diagram

References

1. Smith, O.J. Posicast Control of Damped Oscillatory Systems. *Proc. IRE* **1957**, *45* , 1249–1255. [CrossRef]
2. Singer, N.C; Seering, W.P. Preshaping Command Inputs to Reduce System Vibration. *ASME J. Dyn. Syst. Meas. Control* **1990**, *112*, 76–82. [CrossRef]
3. Singhose, W. Command Shaping for Vibration Reduction: A Review of the First 50 Years. *Int. J. Precis. Eng. Manuf.* **2009** *10*, 153–168. [CrossRef]
4. Chang, C.-S; Singhose, W. Input Shaping for a Flexible Spacecraft Docking Experiment. *J. Guid. Control. Dyn.* **2006**, *29*, 1152–1158.
5. Singhose, W.; Pao, L. A Comparison of Input Shaping and Time-Optimal Flexible Body Control. *Automatica* **1997**, *33*, 1393–1400. [CrossRef]
6. Heckman, C.R; Lawrence, J.R. Input Shaping Applied to Nonlinear Systems with Frictional Effects. In Proceedings of the ASME International Design Engineering Technical Conferences & Computers and Information in Engineering Conference (IDETC/CIE), Brooklyn, NY, USA, 3–6 August 2008.
7. Lawrence, J.; Singhose, W.E.; Hekman, K. An Analytical Solution for a Zero Vibration Input Shaper for Systems with Coulomb Friction. In Proceedings of the American Control Conference, Anchorage, AK, USA, 8–10 May 2002; pp. 4068–4073.
8. Meirovitch, L. *Fundamentals of Vibrations*, International ed.; Mechanical Engineering Series; McGRALL-HILL: New York, NY, USA, 2001.
9. Den Hartog, J.P. *Mechanical Vibrations*, 4th ed.; McGraw-Hill: New York, NY, USA, 1956.
10. Jhonson, K.L. *Contact Mechanics*; Clarendon: Oxford, UK, 1985.
11. Johnson, K.L. *Contact Mechanics*; Cambridge University Press: Cambridge, UK, 1987.
12. Timoshenko, S.P; Goodier, J.N. *Theory of Elasticity*, 3rd ed.; McGraw-Hill: New York, NY, USA, 1970.
13. Arnell, R.D.; Davies, P.B.; Halling, J.; Whomes, T.L. *Tribology Principles and Desing Applications*; Springer: Berlin/Heidelberg, Germany, 1993.
14. Wang, R.; Zhang, J. *Transfer Matrix Method for Multibody Systems: Theory and Applications*; John Wiley & Sons: Singapore, 2019.
15. Rappole, B.W.; Singer, N.C.; Seering, W.P. Multiple-Mode Impulse Shaping Sequences for Reducing Residual Vibrations. In Proceedings of the 23rd Biennial Mechanism Conference, Minnepolis, MN, USA, 11–14 September 1994; pp. 11–16.
16. Kang, C.G.; Kang, B.B. Multi-mode input shapers for eliminating residual vibrations. *JMST Adv.* **2024**, *6*, 247–256. [CrossRef]
17. Hekman, K.; Lawrence, J.; Singhose, W.; Input Shaping for a PD Position Controller Under Coulomb Friction. In Proceedings of the XV IFAC World Congress, Barcelona, Spain, 21–26 July 2002.
18. Hekman, K.; Singhose, W.E.; Lawrence, J. Input Shaping with Coulomb Friction Compensation on a Solder Cell Machine. In Proceedings of the American Control Conference, Boston, MA, USA, 30 June–2 July 2004; pp. 728–733.
19. Lawrence, J.; Singhose, W.E.; Hekman, K. Friction-Compensating Command Shaping for Vibration Reduction. *J. Vib. Acoust.* **2005**, *127*, 307–314. [CrossRef]

Disclaimer/Publisher's Note: The statements, opinions and data contained in all publications are solely those of the individual author(s) and contributor(s) and not of MDPI and/or the editor(s). MDPI and/or the editor(s) disclaim responsibility for any injury to people or property resulting from any ideas, methods, instructions or products referred to in the content.